New approach to determine aerosol optical depth from combined CALIPSO and CloudSat ocean surface echoes

Damien Josset, Jacques Pelon, Alain Protat, Cyrille Flamant

New approach to determine aerosol optical depth from combined CALIPSO and CloudSat ocean surface echoes

D. Josset,[1] J. Pelon,[1] A. Protat,[2] and C. Flamant[1]

Received 30 January 2008; revised 24 March 2008; accepted 9 April 2008; published 21 May 2008.

[1] Backscatter lidar observations such as those provided by the CALIPSO mission are expected to give complementary information to long-used radiometric observations for aerosol properties characterization important to climate and environment issues. However, retrieving aerosol optical depth (AOD) and profiling the aerosol extinction cannot be done accurately applying a standard inversion procedure to the backscatter lidar measurements, without a precise knowledge of aerosol properties on the vertical. The objective of this first study is to propose a new approach to quantify the AOD over the ocean combining the surface return signals from the lidar and radar onboard the CALIPSO and CloudSat platforms, respectively. Taking advantage of the satellite formation within the AQUA-train, first comparisons of AODs retrieved with our method and MODIS ones at tropical latitudes show an overall bias smaller than 1%, and a standard deviation of about 0.07. These first results are presented and error sources are discussed. **Citation:** Josset, D., J. Pelon, A. Protat, and C. Flamant (2008), New approach to determine aerosol optical depth from combined CALIPSO and CloudSat ocean surface echoes, *Geophys. Res. Lett.*, *35*, L10805, doi:10.1029/2008GL033442.

1. Introduction

[2] The aerosol impact on climate is still a major uncertainty as emphasized in the last report of the International Panel on Climate Change. To improve our knowledge in this area, accurate measurements of aerosol optical properties must be performed to better understand their impact. Recently, first lidar observations have been made available from the CALIPSO mission [*Winker et al.*, 2003]. However, up to now lidar inversion algorithms remain stand-alone ones. In this study, we show we can take advantage of the A-Train synergetic observations, using the ocean surface echo as obtained by the lidar CALIOP of the CALIPSO mission, and the radar (CPR) of the CloudSat mission [*Stephens et al.*, 2002]. Using a relationship between the surface return signals for CALIOP and CPR instruments and correcting for the atmospheric transmission at radar wavelength (3.1 mm, frequency 94 GHz), the atmospheric transmission at lidar wavelengths can be retrieved to derive aerosol optical depth (AOD). We apply this method, hereafter called CALIPSO-CloudSat surface reflectance method (CCSRM) to CALIOP measurements at 0.532 μm on a few case studies to retrieve the AOD. Comparisons with MODIS retrievals at 0.55 μm are made at tropical latitudes for validation of the method. In a first part we analyze the method applicable to both lidar and radar instruments, discussing error sources. We then present calibration analysis and results obtained on 4 case studies, ending with a few perspectives.

2. Analysis Principle

2.1. Surface Reflectance Model

[3] The analysis of the ocean surface reflectance has been the subject of many studies for both lidar and radar observations [*Cox and Munk*, 1954; *Barrick*, 1968; *Bufton et al.*, 1983; *Flamant et al.*, 1998; *Menzies et al.*, 1998; *Queuffeulou et al.*, 1999; *Horstmann et al.*, 2003; *Lancaster et al.*, 2005; *Li et al.*, 2005]. The off-nadir angles of CloudSat and CALIPSO observations used here are equal to 0.16° and 0.3°, respectively. With platforms pointing stabilities better than 0.1°, the surface reflectance angular dependence is less than 1% for angles smaller than 0.5° and wind speeds larger than 3 m/s [*Bufton et al.*, 1983] and will be neglected, leading to simplifications in the formulations of the radar and lidar surface reflectance.

[4] Over the ocean, the normalized surface scattering cross section $\sigma_{SR,L}$ (subscript S for surface, while R and L express the dependence with radar and lidar wavelengths, respectively) for a nadir pointing can be written to the first order [*Barrick*, 1968; *Bufton et al.*, 1983]:

$$\sigma_{SR,L} = kC_{R,L}\frac{\rho_{0R,L}}{\langle S^2\rangle} \quad (1)$$

$\langle S^2\rangle$ is the variance of the wave slope distribution formed at the surface by wind stress [*Cox and Munk*, 1954]. The parameter $\rho_{0R,L}$ is the Fresnel reflectance coefficient (ρ_{0R} = 0.41 at 20°C for 3.1 mm radar measurements, and ρ_{0L} = 0.020 for lidar observations at 0.53 μm). $C_{R,L}$ is a coefficient indicative of reflectance modification at radar (lidar) wavelength taking into account diffraction induced by the size of the surface elements linked to surface waves [*Li et al.*, 2005]. For lidar measurements, C_L also contains the reflectance modification due to foam formation [*Koepke*, 1984; *Flamant et al.*, 2003]; k express the impact of the atmosphere vertical stability on the interaction between wind and surface waves [*Shaw and Churnside*, 1997; *Flamant et al.*, 2003]. $C_{R,L}$ should include a wind speed dependent correction with angle for non near-nadir observations.

[5] The wavelength of the capillary waves ranges from 1 mm (viscous dissipation scale) to a few cm [*Phillips*, 1977]. As the lidar wavelength is much smaller, diffraction leads to a negligible contribution to C_L. Foam, however,

[1]Université Pierre et Marie Curie, SA/IPSL, Paris, France.
[2]CETP/IPSL, Vélizy-Villacoublay, France.

0094-8276/08/2008GL033442

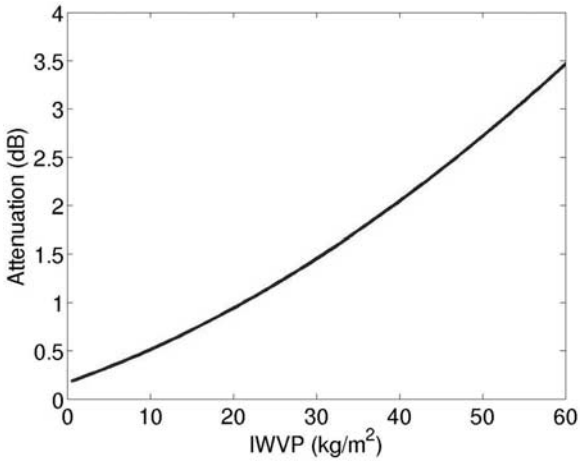

Figure 1. Single path attenuation (in dB) due to water vapor as a function of the integrated water vapor path [*Lhermitte*, 1987].

significantly modifies the surface scattering cross-section for winds larger than 10 m/s [*Koepke*, 1984; *Menzies et al.*, 1998; *Flamant et al.*, 2003], and we can write the modification coefficient C_L in (1) as

$$C_L = 1 + W\left[\rho_w \frac{4\langle S^2\rangle}{\rho_{0L}} - 1\right] \quad (2)$$

W is the area covered by white caps and ρ_w is their reflectance, taken to be constant and equal to 0.22 [*Koepke*, 1984]. W varies as a function of a power law of wind speed [*Flamant et al.*, 2003]. $\langle S^2\rangle$ can be expressed as linearly depending on wind speed [*Cox and Munk*, 1954; *Flamant et al.*, 2003]. In a domain where the surface wind is small, W is close to 0 and one can neglect the term in W in (2), so that $C_L = 1$. C_L is increasing with wind speed, but stays smaller than 1.1 for winds up to 15 m/s.

[6] As radar wavelength is larger than viscous scale, diffraction effects should be taken into account. *Li et al.* [2005] adjusted measurements to calculations as in (1) using $k = 1$. They found a square root value of C_R equal to 0.88 ± 0.16, for wind speed between 3 and 10 m/s.

2.2. Radar Equation

[7] The attenuated normalized scattering cross-section at radar wavelength $\sigma_{SR,att}$ (subscript att for attenuated) is σ_{SR} in (1) attenuated by the two-way atmospheric transmission T_{AR}^2 (subscript A for atmosphere) [*Li et al.*, 2005]. Attenuation at 94 GHz in clear air is caused by oxygen and water vapor absorption [*Lhermitte*, 1987]. The transmission loss linked to water vapor is given in Figure 1 (in dB) as a function of the integrated water vapor path (IWVP). In the tropical regions, where IWVP can reach 60 kg/m^2, a correction factor between 3 and 4 is needed to correct the transmission term T_{AR}^2, whereas it is only 1.5 at mid-latitudes (contents smaller than 20 kg/m^2). Error on IWVP will thus produce larger errors in the surface return signal in the tropics, as discussed below. Attenuation by oxygen is small (lower than 0.2 dB), and correction using CALIPSO pressure and temperature ancillary data, leads to a very small residual error, which will be further neglected.

2.3. Lidar Equation

[8] The lidar equation relates the signal detected to the atmospheric backscattering coefficient β_{AL} (m^{-1} sr^{-1}) as a function of distance. After calibration is performed (normalization to molecular scattering between 30 and 34 km for CALIOP), the attenuated backscattered coefficient $\beta_{AL,att}$ (m^{-1} sr^{-1}) is derived from the measured signal attenuated by atmospheric absorption and scattering. To account for both molecular and aerosol attenuation, the atmospheric transmission can be written as $T_{AL}^2 = T_{AmolL}^2\, T_{AaerL}^2$, where subscripts refer to each contribution. At the ocean surface, $\beta_{AL,att}$ is proportional to σ_{SL}. In order to reduce the error in the determination of the lidar signal peak at the surface due to sampling, we will here consider the integral of the backscattering coefficient (performed 180 m above and 360 m below the altitude of the signal maximum), defined as $\gamma_{SL,att}$ (sr^{-1}). Both the reflectance of the surface and the scattering due to sub-water, suspended material and bubble formation are contributing to $\gamma_{SL,att}$ [*Bufton et al.*, 1983]. Including all these contributions in a single term, we can write

$$\gamma_{SL,att} = C_S \frac{\sigma_{SL}}{4\pi} T_{AmolL}^2 T_{AaerL}^2 \quad (3)$$

C_S is the coefficient linking between $\gamma_{SL,att}$ and the normalized surface scattering cross-section which includes additional sub-water scattering. In the range from 1 to 1.1 at 0.53 μm for wind speeds smaller than 10 m/s and low organic particulate load, it may need further attention in specific areas as subsurface contribution is depending on location and season [*Morel and Prieur*, 1977].

2.4. Analysis From Combined Lidar-Radar Equations

[9] Combining radar and lidar equations (1) and (3) one obtains the relationship between $\gamma_{SL,att}$ and $\sigma_{SR,att}$ as

$$\gamma_{SL,att} = \frac{C_t}{4\pi}\left[\frac{\rho_{0L}}{\rho_{0R}}\right]\frac{{T_{AaerL}}^2}{{T_{AR}}^2}\sigma_{SR,att} \quad (4)$$

$C_t = C_S(C_L/C_R)T_{AmolL}^2$ can be considered as an effective calibration coefficient for the developed method, assuming all terms are constant including foam and subsurface contributions as discussed above. Ct should be close to 1.1 in this case. The AOD $\tau_{AaerL,R} = -\ln(T_{AaerL,R})$ can be written from (4) as

$$\tau_{AaerL} = \tau_{AR} + \frac{1}{2}\ln\left(\frac{\rho_{0L}\sigma_{SR,att}}{4\pi\rho_{0R}\gamma_{SL,att}}\right) + \frac{1}{2}\ln C_t \quad (5)$$

[10] As discussed in next section, we propose, in order to reduce the uncertainty on τ_{AaerL}, to adjust the coefficient C_t applying (4) to observations in a reference region. From this expression, usable at all lidar wavelengths, one can derive the error on AOD as

$$\delta\tau_{AaerL} = \delta\tau_{AR} + \frac{1}{2}\left(\left|\frac{\delta\sigma_{SR,att}}{\sigma_{SR,att}}\right| + \left|\frac{\delta\gamma_{SL,att}}{\gamma_{SL,att}}\right| + \left|\frac{\delta C_t}{C_t}\right|\right) \quad (6)$$

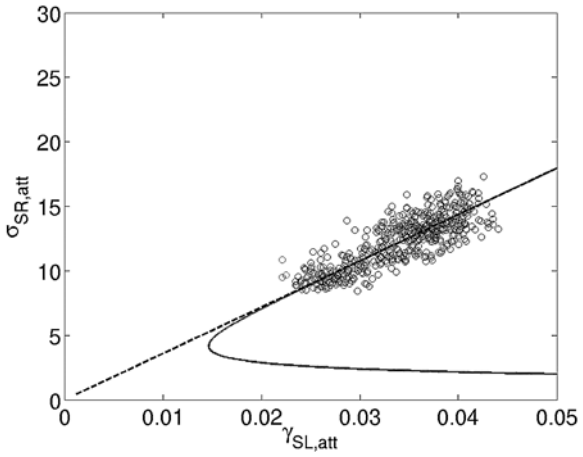

Figure 2. The parameter $\sigma_{SR,att}$ at mid-latitudes over the Atlantic Ocean (May 2007), in clear and dry air conditions, as a function of $\gamma_{SL,att}$ at 532 nm. The dashed line is obtained from a linear fit to the data including the origin, and the solid curve includes the whole dependence on wind speed with foam production using the fitted calibration coefficient C_t (see text).

[11] Error on the AOD $\delta\tau_{AaerL}$ is thus directly depending on the error on the water vapor absorption at radar wavelength $\delta\tau_{AR}$, on calibration error δC_t, lidar and radar change in calibration and signal noise $\delta\sigma_{SR,att}$, $\delta\gamma_{SL,att}$, with respect to the reference region. Error due to molecular density change between reference and observation areas is small and will be neglected in this first approach. As the k factor vanishes in (4), atmospheric stability does not directly contribute to the error budget.

2.5. Calibration

[12] In order to check the validity of expression (4), we have first looked to areas with low aerosols contents at high latitude, to minimize uncertainties in aerosols and water vapor corrections. Level 1 CloudSat release 4.0 and CALIPSO version 1.10 and 1.20 data (0.532 μm, parallel polarization) have been used. CloudSat data are used at maximal horizontal resolution (nominal footprint of 1.4 km across by 2.5 km along track). The horizontal resolution of CALIPSO data correspond to a footprint of about 70 m at the surface every 333 m, on a shot to shot basis.

[13] Figure 2 shows the distribution of $\gamma_{SL,att}$ (532 nm) as a function of $\sigma_{SR,att}$, over the Atlantic Ocean, near 45°N in May 2007 for wind speed between 3 and 10 m/s. The AOD, varying between 0.05 and 0.1 at 550 nm, has been corrected using MODIS/AQUA measurements (product MYD04, 10 km horizontal resolution level 2 collection 5). Transmission at radar wavelength due to integrated water vapor path (IWVP) was also corrected using infrared (product MYDO5, 5 km and 1 km horizontal resolution) measurements. Indeed, two IWVP MODIS products corresponding to visible and infrared channels are available. Comparing them at the same 1 km resolution, it was found that significant differences were observed within cloud structures, and outside these regions a small bias of about 2 kg/m^2 was evidenced. Dispersions were much smaller. As day and night analyses are aimed at, only the IR product was considered in this study. The molecular optical depth τ_{AmolL} calculated from CALIPSO meteorological data, equal to 0.11 is accounted for in the calculation of C_t.

[14] We have reported in Figure 2 the best linear fit to the data, which includes the origin, as in (4) assuming a constant value of C_t. From the regression made, a value of C_t equal to 0.7 was obtained with an accuracy better than 10%. This value is smaller than what is expected. However, lidar and radar calibration errors may explain this difference (for daytime observations as large as 20–30% for lidar release 1.20 (D. Winker, private communication, 2007), and comparable or even larger for radar release 4.0 (S. Tanelli, private communication, 2007)). The error in τ_{AR} is about 0.02 for a 10% error (this is the error expected from MODIS observations [*Seemann et al.*, 2003]) on a IWP equal to 20 kg/m^2 as observed here. The dispersion is due to noise in the measurements themselves. Using the value of C_t obtained from this fit and the full dependence of C_t (through C_L) as a function of wind speed, allows to get the overall expected variation curve of $\gamma_{SL,att}$ (σ_{SR}), as reported in Figure 2. As seen in Figure 2, the observations belong to a domain of linearity where $\gamma_{SL,att}$ is larger than 0.02 sr^{-1} (wind speed smaller than 10 m/s). No saturation of the

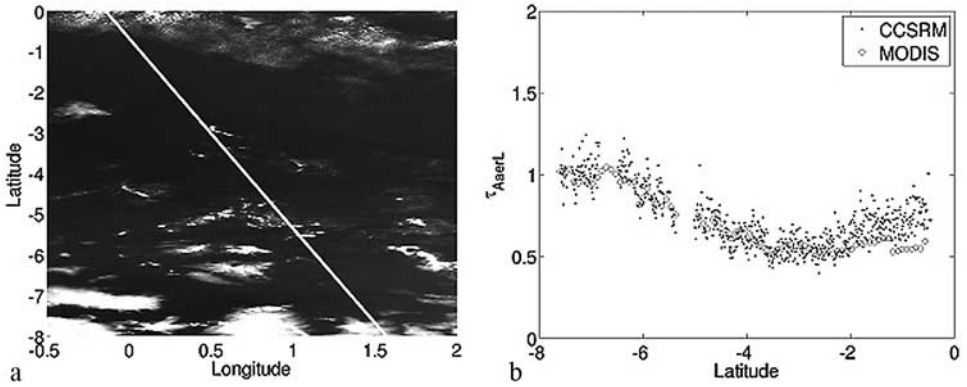

Figure 3. (a) MODIS composite showing the spatial distribution of clear and cloudy air masses close to the CALIOP track (solid line). Clear areas are indicative of the presence of low level clouds. (b) AOD as retrieved on CALIPSO track at 1 km horizontal resolution using CCSRM compared to MODIS (MYD04 product at 10 km horizontal resolution), for the 13 August 2006 at 13:40 UT. Missing points correspond to cloud screening.

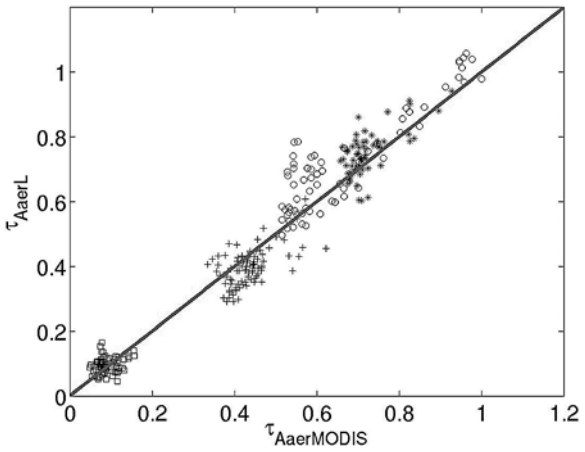

Figure 4. Comparison of AODs retrieved with CCSRM and MODIS data for the 3 tropical cases (circles are for 13 August, stars are for 17 August, pluses are for 20 August) over the Gulf of Guinea. The 16 May 2007 data over the Atlantic Ocean used for reference are also reported (squares corresponding to values smaller than 0.20). Horizontal resolution is 10 km for all data.

lidar signal is detected in the observations (expected to happen for $\beta_{AL,att}$ close to 10^{-3} m^{-1} sr^{-1} and $\gamma_{SL,att}$ larger than 0.05 sr^{-1}, which is corresponding to a wind speed smaller than 3 m/s). The minimum σ_{SL} value of 7 and the minimal value of $\gamma_{SL,att}$ of 0.02 sr^{-1}, as well as a wind speed values between 3 and 10 m/s, thus determine the domain of validity of this method (as plotted in Figure 2) to keep the overall error on calibration smaller than 15%.

3. Aerosol Optical Depth Retrieval

3.1. The Studied Cases

[15] We consider here data obtained over the Guinea Gulf area during August 2006, in a zone between latitudes 30°S and 5°N, longitudes 20°W and 10°E. We have chosen 3 cases of biomass burning aerosol outbreak episodes with low cloud fraction over the ocean (broken stratocumulus). Cloud screening was applied on CALIPSO data. The corresponding MODIS granules used for the comparisons are taken on 08/13/06 at 13:40 UT, 08/17/06 at 13:15 UT, and 08/20/06 at 13:45 UT. The RGB MODIS composites, reported in Figure 3a for the case of 13 August, show that, on the selected days, measurements were done in areas with small broken clouds between cloud layers.

3.2. Results

[16] The results of the analysis made on the selected cases and comparison with the closest MODIS pixel (Aqua aerosol 550 nm MYD04 product) are reported in Figures 3 and 4. As shown in Figure 3, the overall variation of the AOD obtained from CCRSM analysis along the track passing the 13 August 2006 over the Gulf of Guinea at 13:40 UTC is close to MODIS retrieval. Retrievals of MODIS are smoother, which is consistent with a 10 km resolution, as compared to the 1 km analysis of the present CALIOP/CloudSat data. Higher optical depths in southern part are well observed by both methods. The two retrievals significantly differ in the northern part (difference as high as 0.2) north of 2°S. Part of this bias could come from an error in water vapor attenuation near the cloud structure (Figure 3a), change in C_t, or less probably to lidar (radar) calibration variation with respect to the reference area. In the tropics, the observed bias is expected to have its main origin in the correction of the IWVP. An error on IWVP equal to 4 kg/m^2 (about 10% of the measured IWVP for the studied cases) in the tropics, would lead to an error of about 0.06 on the AOD.

[17] Figure 4 shows the distribution of the AOD measured at tropical latitudes (between 10°S and 1°N) as compared to MODIS ones, for the 3 days corresponding to the selected cases over the Gulf of Guinea. Results were averaged over MODIS aerosol 10 km grid to increase the meaningfulness of the comparison. Averaging reduces the dispersion, as compared to Figure 3b, but the previously discussed local biases remain, namely on larger values near 1°S for 13 August 2006 (circles in Figure 4). The overall bias is however small between CCSRM and MODIS retrievals. The calibration method used appears to be efficient, even though a simplified approach has been used. Mid-latitude results are also reported (AODs smaller than 0.25), but as the analysis performed in the calibration procedure to retrieve C_t includes the correction of MODIS AOD, coherence is necessarily obtained between MODIS and CCSRM data. The overall mean slope shows a small bias about 0.58%, which does not appear to be significant. Standard deviation is rather high, about 0.07, but is quite encouraging considering possible errors due to water vapor variability and calibration uncertainty. Improved results are expected at mid-latitudes.

4. Conclusion

[18] The method proposed here to retrieve the AOD from the analysis of the ocean surface echo of CALIOP and CPR has proven to be promising. In the domain of linearity dependence of lidar and radar surface returns, it does not require any knowledge on surface wind speed, and atmospheric stability as previously needed [*Flamant et al.*, 1998, 2003]. It has been successfully tested on 3 cases at tropical latitudes for which water vapor correction is important, and allowed to get a very good agreement with MODIS AOD retrieval. This method working for day and night operation, proves to be fairly robust for wind speeds between 3 and 10 m/s. It allows efficient screening of small low level clouds (which reflectance can be mixed with aerosol one in large pixels using radiometry), as it can be performed at the level of the lidar spot size (70 m). The screening in the tested cases was in good agreement with MODIS one performed at 1 km resolution. This method will be further applied to a larger number of CALIPSO-CloudSat observations over the globe, and should also be applicable to measurements at other lidar wavelengths, as for example in the next lidar-radar mission EarthCare planned by the European Space Agency.

[19] **Acknowledgments.** We would like to thank the Centre National d'Etudes Spatiales (CNES) and THALES ALENIA-SPACE for supporting one of us (D. Josset). We acknowledge the anonymous referees for helpful comments and O. Bock, S. Tanelli, Y. Hu, W. Hunt, K. Powell, M. Vaughan, D. Winker, and F.-M. Bréon for fruitful discussions, as well as P. Genau, N. Pascal, and J. Tarniewicz for their help in the data preparation, and U.S. (http://www-calipso.larc.nasa.gov, http://cloudsat.cira.colostate.edu, http://ladsweb.nascom.nasa.gov/) and French (http://www.icare.univ-lillel.fr) archive centers.

References

Barrick, D. E. (1968), Rough surface scattering based on the specular point theory, *IEEE Trans. Antennas Propag.*, *AP16*(4), 449–454.

Bufton, J. L., F. E. Hoge, and R. N. Swift (1983), Airborne measurements of laser backscatter from the ocean surface, *Appl. Opt.*, *22*(17), 2603–2618.

Cox, C., and W. Munk (1954), Measurement of the roughness of the sea surface from photographs of the Sun's glitter, *J. Opt. Soc. Am.*, *44*(11), 838–850.

Flamant, C., V. Trouillet, P. Chazette, and J. Pelon (1998), Wind speed dependence of atmospheric boundary layer optical properties and ocean surface reflectance as observed by airborne backscatter lidar, *J. Geophys. Res.*, *103*(C11), 25,137–25,158.

Flamant, C., J. Pelon, D. Hauser, C. Quentin, W. M. Drennan, F. Gohin, B. Chapron, and J. Gourrion (2003), Analysis of surface wind and roughness length evolution with fetch using a combination of airborne lidar and radar measurements, *J. Geophys. Res.*, *108*(C3), 8058, doi:10.1029/2002JC001405.

Horstmann, J., H. Schiller, J. Schultz-Stellenfleth, and S. Lehner (2003), Global wind speed retrieval from SAR, *IEEE Trans. Geosci. Remote Sens.*, *41*(10), 2277–2286.

Koepke, P. (1984), Effective reflectance of oceanic whitecaps, *Appl. Opt.*, *23*, 1816–1824.

Lancaster, R. S., J. D. Spinhirne, and S. P. Palm (2005), Laser pulse reflectance of the ocean surface from GLAS satellite lidar, *Geophys. Res. Lett.*, *32*, L22S10, doi:10.1029/2005GL023732.

Lhermitte, R. (1987), A 94 GHz Doppler radar for cloud observations, *J. Atmos. Oceanic Technol.*, *4*, 36–48.

Li, L., G. M. Heymsfield, L. Tian, and P. E. Racette (2005), Measurements of ocean surface backscattering using an airborne 94-GHz cloud radar—Implication for calibration of airborne and spaceborne W-band radars, *J. Atmos. Oceanic Technol.*, *22*, 1033–1045.

Menzies, R. T., D. M. Tratt, and W. H. Hunt (1998), LITE Measurements of sea surface directional reflectance and the link to surface wind speed, *Appl. Opt.*, *37*, 5550–5559.

Morel, A., and L. Prieur (1977), Analysis of variations in ocean color, *Limnol. Ocean.*, *22*(4), 709–722.

Phillips, O. M. (1977), *The Dynamics of the Upper Ocean*, 2nd ed., Cambridge Univ. Press, New York.

Queuffeulou, P., B. Chapron, and A. Bentamy (1999), Comparing Ku-band NSCAT scatterometer and ERS-2 altimetter winds, *IEEE Trans. Geosci. Remote Sens.*, *37*(3), 1662–1670.

Seemann, S. W., J. Li, W. P. Menzel, and L. E. Gumley (2003), Operational retrieval of atmospheric temperature, moisture, and ozone from MODIS infrared radiances, *J. Appl. Meteorol.*, *42*(8), 1072–1091.

Shaw, J. A., and J. H. Churnside (1997), Scanning-laser glint measurements of sea-surface slope statistics, *Appl. Opt.*, *36*, 4202–4213.

Stephens, G. L., et al. (2002), The CloudSat Science Team, The CloudSat mission and the A-Train, *Bull. Am. Meteorol. Soc.*, *83*(12), 1771–1790.

Winker, D. M., J. Pelon, and M. P. McCormick (2003), The CALIPSO mission: Spaceborne lidar for observation of aerosols and clouds, *Proc. SPIE*, *4893*, 1–11.

C. Flamant, D. Josset and J. Pelon, Université Pierre et Marie Curie, SA/IPSL, 4, Place Jussieu, B102, F-75252 Paris Cedex 05, France. (damien.josset@aero.jussieu.fr)

A. Protat, CETP/IPSL, 10-12 Avenue de l'Europe, F-78140 Vélizy-Villacoublay, France.